The dynamics of plasma-surface interaction

Gou, F.

Chapter 5

Theoretical modeling of energy redistribution and stereodynamics in CF scattering from Si(100) under grazing incidence

Abstract: We have simulated CF scattering from Si (100) using the molecular dynamics method. Translational energy loss spectra are presented. The shape of the energy loss distribution as a result of internal energy release is analyzed. At the classic turning point, the internal energy of the molecule is mainly in form of rotational energy. The strong rotational excitation results in additional molecule-surfaces interactions during the latter half of the collision. These additional collisions permit some molecules that initially gain internal energy exceeding the bond strength to ultimately survive the collision process via rotational de-excitation. The rotational motion exhibited by surviving molecules is determined by the combination of the molecular axis orientation and the local surface structure during the collision process. The rotation planes of the surviving molecules are preferentially aligned with the surface normal (cartwheel-like and propeller-like motions). In this study, propeller-like motion of the surviving molecules is observed for the first time. The majority of surviving molecules exhibit a cartwheel-like motion. However, molecules that gain a propeller-like rotation exhibit a much better alignment of their planes of the rotation compared with molecules exhibiting cartwheel-like motion.

5.1 Introduction

Understanding the interaction of gas-phase molecules with solid surfaces has relevance for a wide range of technologically important processes [1-4], including catalysis, surface modification, etching and passivation. The interaction can be broadly split into two components, the electronic and the mechanical. Invariable both components are operative, but the relative importance varies depending on the particular molecules and surfaces involved and on the initial state of the molecule. Investigating the interaction of molecules with surfaces is challenging when compared to atom-surface studies. Molecular interaction contains the added possibilities of excitation of internal modes and/or dissociation. Given the extra complexity, it can often be difficult to experimentally distinguish the root cause of a particular observation. In this regard, computer simulation is a valuable tool for providing explicit information about the dynamics of molecules over short (picosecond) time scales and

is ideally suited to the microscopic study of molecule-surface interaction and related phenomena [5; 6].

Previously, simulations have indicated that the degree of collision induced dissociation for grazing incident molecules is primarily determined by the normal energy and is only weakly dependent on the parallel energy [7]. Under grazing conditions, molecules with a large total energy can have normal energies of less than 10 eV. Such energies are typical for the activation of chemical reactions at surfaces. As a consequence, results obtained for grazing incidence (e.g. internal energy uptake and dissociation rate as a function of normal energy) may be qualitatively applicable to less grazing geometries. This is highly advantageous when seeking to study the interaction of low energy (1-50 eV) particles with surfaces. A relative lack of adequate beam sources and efficient detectors hampers experimental investigation in this energy range. Provided normal-energy scaling at grazing incidence can be demonstrated to adequately mimic the dynamics of low energy particles at normal incidence, then more efficient sources and detectors can be applied to the investigation of such low energy particle-surface interactions. Of course, when such an experimental approach is adopted [8; 9], it is necessary to rigorously investigate the applicability and limits of normal energy scaling.

In the past decades much theoretical work has been done on grazing scattering of homo-nuclear diatomic molecules from metal surfaces [2]. Van den Hoek and Kleyn [10] have performed MD simulations of O_2 scattering from the Ag (111) surface over a range of incidence energies from 1eV to 3 keV. These calculations show that for grazing incidence, both the total energy loss and the dissociation fraction go through a maximum at several 10's of eV incident beam energy before becoming independent of total energy beyond several hundred eV while keeping normal energy fixed. Heiland's group performed classical trajectory calculations of fast N_2 scattering from Pd (111) at grazing incidence, based on ab initio density functional theory calculations[6]. Their results show that the molecule-surface interaction seems to be strongly dependent on the azimuthal direction of incidence and the orientation of the molecular axis. Many studies have focused on the rotational dynamics arising from the scattering. Studies by Gerber et al. have shown a strong preference for rotational inelastic transitions resulting in the vibrational deactivation of I_2 scattering from MgO(100)[11]. Relatively few studies have been performed on scattering of hetero-nuclear molecules from surfaces. Martin et al. have studied the dissociation dynamics and energy transfer processes of NO scattering from GaAs (110) [12]. Trajectory calculations by Polanyi and Wolf show that the initial orientation angle of CO strongly affects the final rotational state and angular distribution [13].

In this paper we present MD simulations of CF molecules scattering from the Si (100) surface in order to gain insight into the mechanism of scattering and CID. The current simulations involve molecules incident on the silicon surface at grazing incidence (<10° with respect to the surface plane). One of the primary motivations for the selection of scattering geometry and surface was work being performed using a grazing-incidence ion scattering apparatus at our laboratory. Such experiments can be utilized for the validation of computer models, which can then be applied to the simulation of surface interactions at different geometries and incident energies. Although the current simulations may not be directly comparable to experimental results (since electronic effects have been wholly neglected), the mechanical collision processes outlined in this paper should none-the-less be operative during molecular scattering (as illustrated by the observation of CID effects in the scattering of CF_3^+ from Ag(111) [14]). In terms of relevance to ion scattering, the current work would be directly applicable to incident ions that are not neutralized or are neutralized to the ground state (e.g. via auger neutralization). Comparison between theory and experiments can be used to derive information on electronic processes based on differences as well as similarities.

Molecules that neutralize to an excited state would have an additional internal energy component that is absent in the current work. Dissociative neutralization is a factor that is completely absent at present.

Experimentally, relatively little beam work has been performed on the interaction of fluorocarbon molecules with surfaces. The main work that has been done has involved the use of ion beams. Koppers et al. have studied the dissociative scattering of CF_3^+ ions from clean and barium covered Ag (111) surfaces [15]. Unsurprisingly, the results showed that dissociation occurs mainly as a result of electronic processes. However, it was noted that the crystal orientation has a measurable influence on dissociation, indicating that impulsive collisions also played a role in fragmenting the incident molecules. Koppers et al. also investigated CF_x^+ (x=1-3) scattering from a liquid perfluoropolyether (PFPE) surface [16; 17]. PFPE is an insulating surface and consequently fragmentation was solely due to collision-induced dissociation (CID). The degree of dissociation was correlated with the number of bonds in the incident molecule. The results suggested that the orientation at impact played an important role in the degree of internal energy uptake (and hence dissociation) of the incident molecules.

Under grazing scattering conditions, the incident particles are very sensitive to the outermost atomic layers of the surfaces. The combination of small perpendicular velocity and large parallel velocity results in incident molecules traveling a long distance close to the surfaces. The use of a well-ordered surface can give rise to 'special' scattering effects. For instance, channeling of atoms by atomic rows on the surface can be observed [9]. In the case of molecular projectiles, the possibility of channeling also exists. In addition, molecular scattering may give rise to experimentally observable effects, either solely due to the molecular orientation (e.g. orientation dependent dissociation [17]) or by the combination of the molecular orientation and the surface structure. In order to properly interpret experimental results, such effects should be accurately identified. Simulation is an ideal tool to check for structural effects in the scattering of molecules. It is trivial to perform calculations with a well-defined starting molecular orientation (equivalent to producing an oriented beam experimentally). Equally, angular distributions, dissociation probability variations and selective excitations of the scattered particles can be readily identified. Of course, observing such effects experimentally may be difficult in many cases. None-the-less simulations can act as a useful indicator of scattering effects that may be experimentally observable.

In the current work we analyze the translational energy loss, the internal energy uptake and the amount of the vibrational and rotational excitation of CF scattered from Si (100). We examine the relationship between dissociation, molecular orientation, orientation of the rotational angular momentum ($\vec{J}$) and the effect of the surface structure and demonstrate that the type of rotational motion exhibited by scattered molecules is closely related to both the initial molecular orientation and the surface structure.

5.2 Description of the molecular dynamics simulation

In this paper we focus on the simulation of CF scattering from Si (100) using a fixed parallel energy of 1500 eV and varying the normal energies ($E_\perp$=Esin2θ_i) from 4 eV to 31 eV. This combination of energies corresponds to incident angles θ_i of between 2.9° and 8.2° with respect to the surface plane. Under such grazing incidence conditions, the scattering mode is expected to change from binary collision between the incident molecules and individual surface atoms to simultaneous multi-body interactions between the molecule and the surface

atoms. Many simulations propose that the binary collision model is still suitable at grazing incidence. However, trajectory analysis shows that the binary collision model is not entirely suitable for the grazing scattering case [5]. Consequently, we have utilized MD simulations to examine the scattering of CF from Si (100) surfaces.

Details of the MD method can be found elsewhere [18], but we briefly describe the procedure here. Molecular dynamics simulations calculate the positions and velocities of a system of atoms by numerically integrating Newton's equation of motion. The net force exerted on each atom is calculated from the gradient of an inter-atomic potential energy function. In our simulation we use a pair potential to describe the intermolecular C-F interaction [19].

$$V_{ij}(r) = A_{ij} \exp(-\lambda_{ij} r_{ij}) - B_{ij} \exp(-\mu_{ij} r_{ij})$$

where A_{ij} and B_{ij} are 909.2022 eV and 219.7799 eV. λ_{ij} and μ_{ij} are 3.7128 $Å^{-1}$ and 2.1763 $Å^{-1}$. The Molière potential is used to describe the interaction of silicon atoms with C and F [20]. We use a spring potential to describe the interaction among the crystal atoms and each crystal atom interacts only with its nearest neighbors [21]. The choice of a spring potential to describe the Si-Si interactions was made in order to reduce the overall computation time. Clearly this is an unphysical description of the way in which the surface atoms interact with each other. However, we believe the use of a spring potential is not significantly detrimental to the computation results due to the incident molecules having a large translational velocity parallel to the surface. As a consequence, the time spent in the vicinity of an individual Si atom is small and the interaction of the molecules with individual silicon atoms is dominated by the initial collision. The subsequent response of the Si atoms occurs after the molecule has left the vicinity and does not influence the trajectory or the energy exchange between the molecule and the surface. Although the energy redistribution within the crystal is not accurately described, this is not relevant to the trajectory of the exciting molecule. Each trajectory is scattered from a 'new' surface, so lattice excitations from one trajectory do not transfer to subsequent molecules.

The use of a spring potential does not permit the sputtering of surface atoms, although this should in principle be possible given the highest normal energy employed (31 eV). Again, due to the large parallel velocity and the use of a fresh surface for each molecule, the neglect of sputtering can be considered a minor omission. If the study were expanded to include surface defect then the issue of sputtering would become more critical. Test trajectories, performed utilizing both Morse [22]and Tersoff potentials [23-25] for the Si-Si interaction, were compared to calculations using the spring potential. There was no significant difference between the molecular distributions observed for the three lattice potentials, supporting the conclusion that a precise description of the Si-Si interaction is not critical for grazing incidence simulations. In order to check the applicability of "normal-energy scaling", some sample calculations were performed using normal incident molecules (no parallel energy). In these cases, the Tersoff Brenner potential was used for the Si-Si interaction.

We use the velocity Verlet scheme with a variable time-step to numerically integrate Newton's equations of motion. For each time-step in the trajectory, pair potentials are summed for atoms within a cut-off distance (R_c = 6Å) of the incident ion from the surface. Given the large surface area required in order to simulate grazing scattering, the use of a cut-off was necessary in order to limit computation time. Both R_c and the integration time step are chosen to achieve an accuracy of better than 0.1% deviation from total energy. Sample calculations were run to confirm that neither increasing Rc nor decreasing the time-step resulted in a significant change in the simulated results. In order to obtain good statistics, at least 10,000 trajectories have been run at each of the incident energies.

The target consists of a "box" containing three layers of atoms. The side of the box facing the incident molecules serves as the unreconstructed Si (100) surface. For the other sides, the atoms are fixed at their equilibrium positions. Atoms inside the box and on the surface are movable under force. The simulated cell was ~160 Å long (in the scattering direction), ~40 Å wide and ~10 Å deep. The surface area was ~6400 $Å^2$. Test simulations were done to ensure that increasing either the number of layers or the number of atoms per layer did not significantly change the simulation results. At the beginning, the crystal atoms are set to their equilibrium positions and then thermally displaced in terms of the Debye model. According to this, uncorrelated Gaussian distributions are assumed for the atomic displacement and the mean square atomic displacement is proportional to T/Θ, where T is the crystal temperature and Θ is the Debye temperature. The velocity components of the crystal atoms are calculated from the Gaussian distribution. To distinguish thermal effects, results are compared to simulations performed at 0 K (no initial lattice vibration included).

The incident CF molecules are initially placed just above the surface (~6 Å) with a random (X, Y) position, referred to one unit cell on the surface. At this point the surface potential is less than 10^{-5} eV. The incoming (θ_i) and outgoing (θ_f) angles are defined with respect to the surface plane. The polar (in-plane) scattering angle (θ) is defined as the sum of θ_i and θ_f. The azimuthal (out-of-plane) scattering angle (ϕ_i) is measured with respect to the scattering plane, which is defined by the incident atom direction and the surface normal. The initial orientation of the molecular axis is chosen randomly for each trajectory, with proper weighting. The initial angular momentum $\vec{J}$ is zero in order to conserve the orientation until impact. The CF molecules have no initial vibrational energy.

In our calculation, the molecular orientation and the rotational motion are specified by two types of angle: the polar orientation angles, θ_o (θ_J), are between the molecular axis (the rotational angular momentum, $\vec{J}$) and the surface plane; the azimuthal orientation angles, ϕ_o (ϕ_J), are between the projection of the molecular axis (the projection of $\vec{J}$) onto the surface and the initial trajectory along the surface, such that ϕ_o = 0˚ and 180˚ correspond to the molecular axis projection($\vec{J}$ projection) being parallel to the initial trajectory. In our simulations, θ_o = 0˚ and 180˚ correspond to the molecular axis being perpendicular to the surface; in these instances, no azimuthal orientation is defined. Figure 1(a) shows the definition of the polar and azimuthal orientations of the molecular axis (θ_o and ϕ_o). Similarly, figure 1(b) shows the definition of the polar and azimuthal angles of the rotational angular momentum vector $\vec{J}$ (θ_J and ϕ_J, respectively). Molecular rotation with θ_J =0˚ and ϕ_J=0˚ is referred to as propeller-like motion (see figure 1 (c)), θ_J =0˚ and ϕ_J= ±90˚ is called cartwheel-like motion (figure 1(d)) and θ_J =90˚ is helicopter-like motion (figure 1(e)). The rotational energy at a certain point is defined as $\vec{J}^{\,2}/2\mu r$, where μ is the reduced mass and r is the bond length of the molecule. The internal energy is calculated as the sum of the relative kinetic energy and the relative potential energy of the molecule.

5.3 Results and discussion

5.3.1 Energy loss distributions and degree of dissociation

We begin by presenting simulated energy loss distributions of the scattered particles for CF incident on Si(100) at four different normal energies ($E_\perp$= 4 eV, 13 eV, 19 eV and 28 eV). In each case the parallel energy was 1500 eV and the surface temperature was 300 K. Increasing the normal energy while maintaining a fixed parallel energy means that the

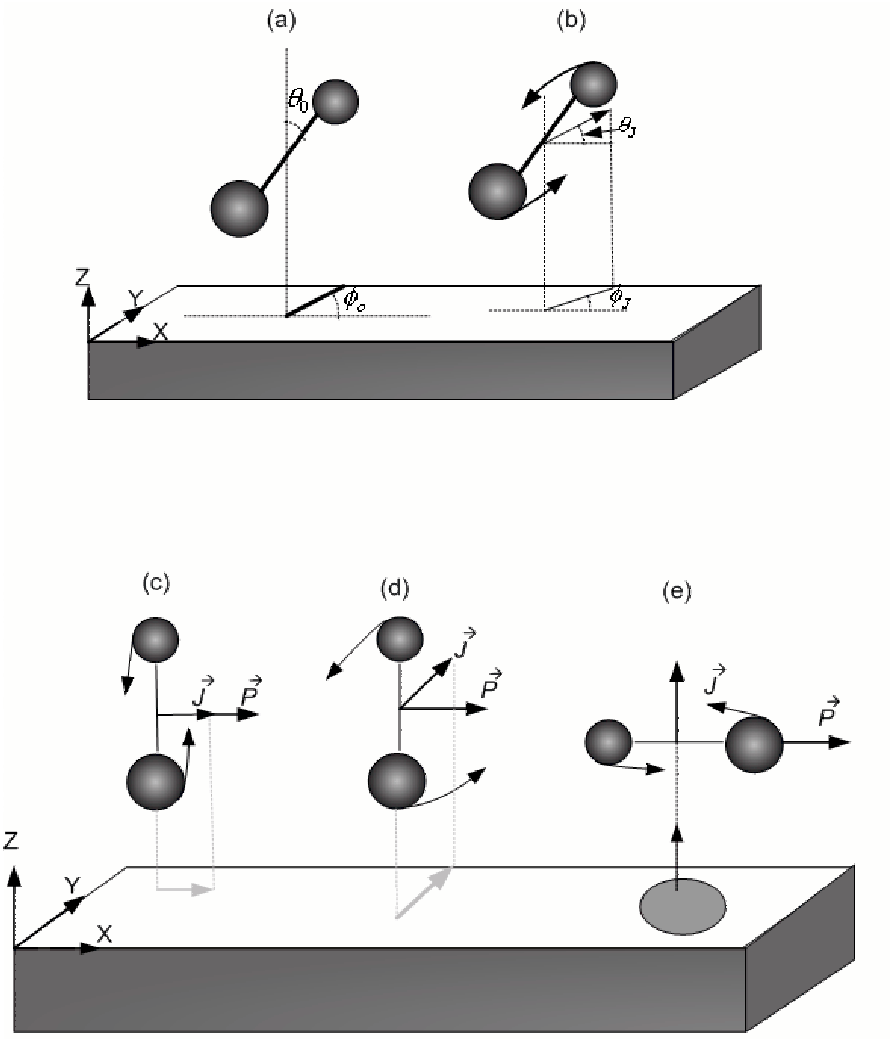

Figure 1: Illustration of the coordinate system used in this paper. (a) Orientation of the inter-nuclear axis. (b) Orientation of the rotational angular momentum. (c) Propeller-like rotation (θ_J =0° and ϕ_J=0°). (d) Cartwheel-like rotation (θ_J =0° and ϕ_J= ±90°). (e) Helicopter-like rotation (θ_J=90°). $\vec{P}$ and $\vec{J}$ are defined as the momentum and angular momentum, respectively.

incidence angle, θ_i (with respect to the surface plane) also increases. The resulting scattered particles are shown in figure 2(a)-(d) as a function of their energy loss.

Each of these distributions is based on the simulation of 30,000 trajectories of CF molecules. The molecules were scattered sequentially, with a randomly selected orientation of the molecular axis as outlined in the previous section. The changes observed in the scattered distribution with increasing normal incidence energy are a result of enhanced energy exchange with the surface.

For $E_\perp$=4 eV (less than the 5.7 eV bond energy of CF) no dissociation occurs as a result of the collision. The peak of the scattered CF distribution corresponds to an energy loss of 2.1 eV. The energy width at half-maximum of the distribution is ~2.5 eV. These values are remarkable low considering the presence of 1500 eV of parallel energy in the incident molecules. Clearly, at grazing incidence the parallel energy is not readily accessible, neither for excitation of the internal modes of the molecule nor for energy exchange with the surface.

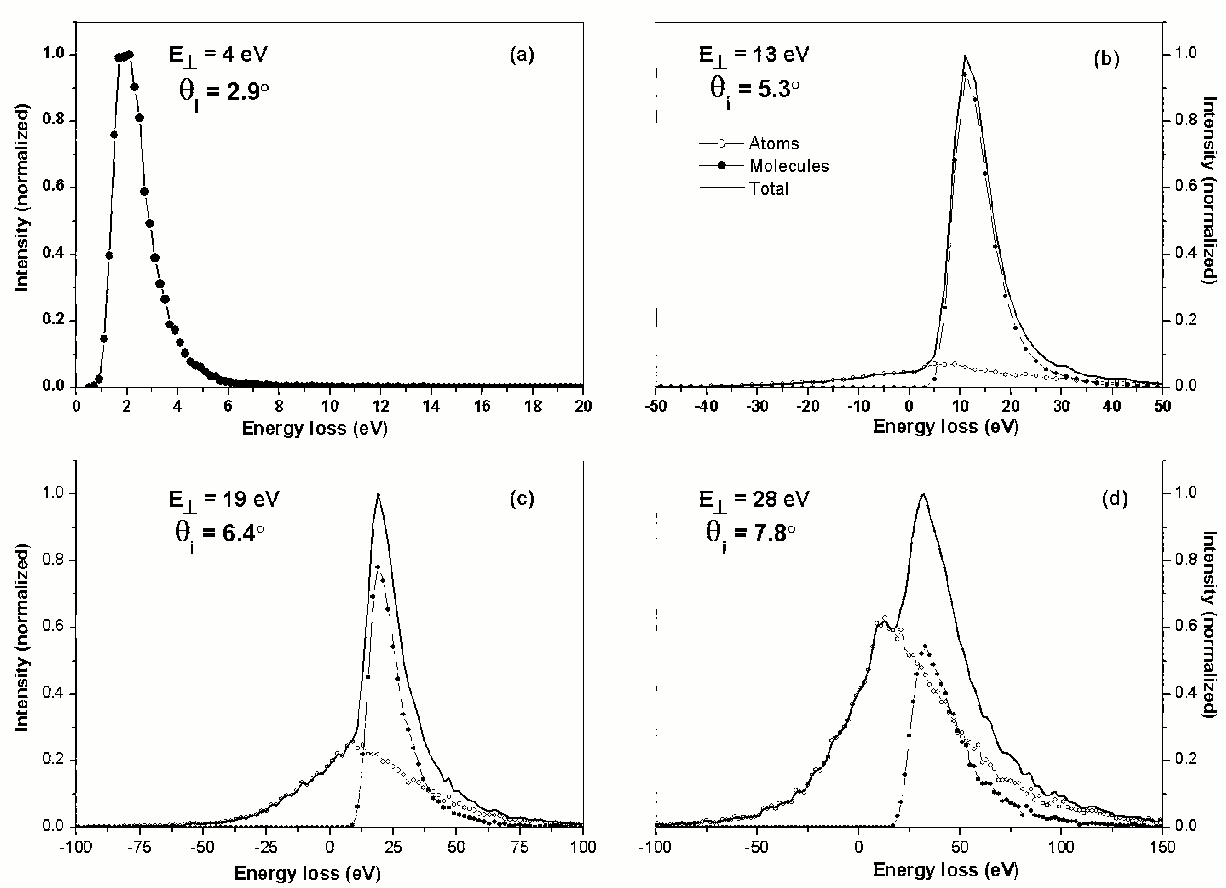

Figure 2: Energy loss of scattered particles (C and F atoms represented by open circles; surviving CF molecules represented by filled circles). $E_{//}$ =1500 eV and surface temperature of 300 K. (a) $E_{\perp}$ = 4 eV (b) $E_{\perp}$ = 13 eV (c) $E_{\perp}$ =19 eV (d) $E_{\perp}$ = 28 eV. The energy gain exhibited by some of the scattered atoms is a consequence of internal energy release in the CM frame when the molecule dissociates (see text for details).

For $E_{\perp}$= 13 eV dissociation becomes evident. As a consequence, the energy loss distribution of the scattered particles contains two parts: one due to scattered molecules, the other due to scattered atoms arising from dissociation. In addition to the overall distribution, the individual distributions of the scattered molecules and scattered atoms are indicated on figure 2(b). The overall distribution is dominated by the contribution from scattered molecules. The molecular distribution has a similar shape to that observed for $E_{\perp}$=4 eV, however the energy loss at maximum intensity is larger and the distribution is broader.

It is found that 13% of the incident molecules dissociate at $E_{\perp}$= 13 eV. The energy loss of the resulting atoms is determined by subtracting the final energy of a scattered atom from the proportion of the initial energy of the molecule that can be assigned to that atom on the basis of its mass. The energy loss distribution of the atoms is very broad and almost symmetric. Some atoms have a final energy that exceeds its initial energy (negative energy loss on the figure). This is a consequence of internal energy release upon dissociation (see details below). In contrast, all scattered molecules have energies lower than the initial energy.

Increasing the normal energy to 19 eV (shown in figure 2(c)) further increases the dissociation rate. At this energy, 35% of the incident molecules dissociate. The atomic component of the scattered distribution is now clearly evident. The shapes of both the atomic and molecular distributions are similar shape to the equivalent distributions observed at $E_{\perp}$=13 eV, but are much broader. In this case, the energy loss at the maximum of the

molecular distribution (~22 eV) exceeds the initial normal energy. This indicates that as the normal energy is increased (less grazing incidence) the parallel energy becomes more accessible to the collision process. However, the total energy loss is still remarkably low compared to the amount of parallel energy in the molecule. When the normal energy is increased to 28 eV (shown in figure 2(d)), about 60% of the molecules dissociate. At this point the components due to scattered molecules and scattered atoms can be clearly distinguished. As before, the increased normal energy results in more energy loss (at maximum) and broader distributions. Note that the maxima of the atom distributions are consistently lower (in energy loss) than those of the corresponding molecule distributions. In the first instance, this is counter-intuitive: the molecules that dissociate (most internal energy uptake/hardest collision) exhibit less cumulative energy loss. Briefly, it is due to the number of interactions between the molecule and the surface atoms influencing both the total energy loss and the survival probability. This point will be addressed later.

The ability of some atoms to exceed their initial energy as a result of dissociation has been observed experimentally, for instance in the case of N_2 scattering from Pd(111) surface [6]. The effect is due to the release of excess internal energy gained during the collision (energy exceeding the bond strength) upon dissociation [26]. This excess energy is released in the molecule's center-of-mass (CM) frame. For a diatomic molecule, assuming the velocity change by the atoms is parallel to the (pre-dissociation) molecular trajectory, the resultant energy of the atoms, observed in the laboratory frame, can be obtained from the following Galilei transformation [27]:

$$E_{m1} = (m_1+m_2)^{-1}(m_1*E_0 + m_2*\varepsilon \pm 2*(m_1.m_2E_0.\varepsilon)^{1/2}) \qquad (1)$$

E_0 is the kinetic energy of molecule before dissociation, m_1 and m_2 are the atomic masses, and ε is the internal energy released from the molecule in the CM frame. There are two solutions to equation 1. The larger value represents the atom that increases its velocity and thus gains energy in the laboratory frame after dissociation; the smaller value represents the other atom, which loses energy in the laboratory frame. Note that for every fragment that gains energy as a result of the dissociation, there is a corresponding fragment that loses energy (hence the broad and relatively symmetric distribution). To illustrate, figure 3 shows the maximum energy change anticipated for the atoms of a CF molecule with E_0=1513 eV as a function of the internal energy released (ε).

We are assuming that the C atom gains energy while the F atom loses energy in the measurement frame. For the purposes of this calculation, the energy released is assumed to already be in the molecule and thus is not extracted from E_0. After dissociation, an internal energy release of between 0-10 eV results in a maximum energy broadening of 0-230 eV for the fragments (difference between the observed energy gain by C and the observed energy loss by the corresponding F). This range is comparable with that of the simulated results shown figure 2. Note that the large energy spread exhibited by the atoms does not imply a large energy exchange with the surface. It is purely a consequence of the excess internal energy in the molecule.

The calculation shown in figure 3 represents the optimum case in which the translational momentum given to the atoms in the CM frame is along the CM momentum of the molecule prior to dissociation. Of course, experimentally there will, almost invariable, be a random distribution of the molecular orientation prior to dissociation. Since the velocity gained by the atoms as a result of internal energy release is independent of the trajectory of the molecule and can be perpendicular to it, the atoms exhibit a broader angular distribution as well as a broader energy distribution when compared to the surviving molecules. The inset on figure 3 shows a comparison between the polar angle distribution of the scattered molecules and scattered atoms. In both cases, the maximum intensity corresponds to the specular scattering

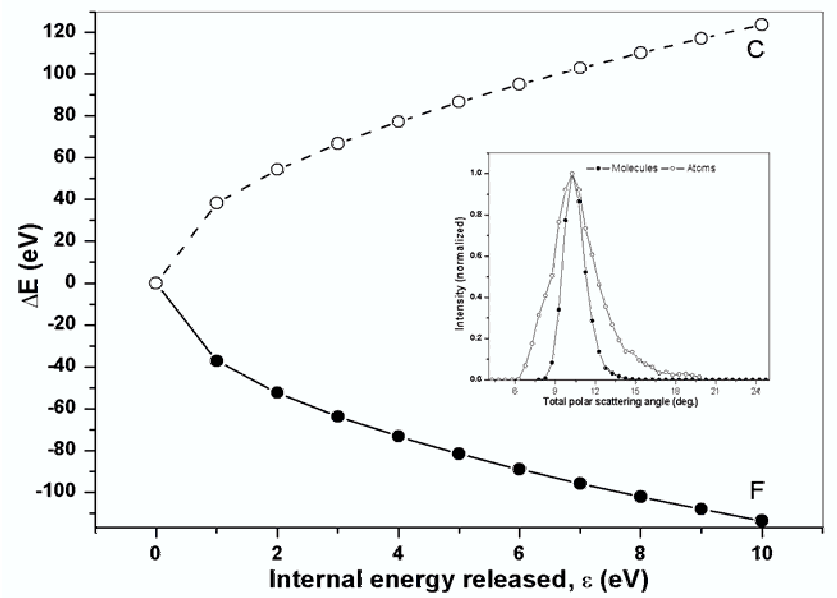

Figure 3: Maximum energy broadening of C and F fragments calculated from equation 1 (see text for details). Inset: polar scattering angle distribution of C and F atoms (open circles) and surviving CF molecules (filled circles). $E_{\perp}$=13 eV; $E_{//}$=1500

direction. However, the angular width of the scattered atoms is substantially broader than that of the molecules.

The energy loss observed and the degree of dissociation are a consequence of the transfer of translational energy from the molecule both to the surface atoms and to the molecule's internal degrees of freedom. Figure 4(a) shows the variation of the averaged internal energy uptake (left ordinate) and the averaged total translational energy loss (right ordinate) as a function of the initial normal energy for molecules that survive the collision. Calculated curves are shown for scattering from a surface at 0 K and at 300 K.

The general behavior observed at the two surface temperatures is the same. With increasing normal energy, more translational energy is lost by the molecules. The scaling with normal energy is not linear. At low normal energies the translational energy loss is less than the normal incidence energy, but this reverses as the normal energy increases (less grazing angles). Hence, the parallel energy becomes increasingly accessible as a function of the increasing angle of incidence. However, even at the largest angle studies the maximum translational energy loss observed represent only ~3.6% of the total initial energy. The translational energy loss at 300 K is consistently greater than that at 0 K. This can be attributed to an increase in the surface roughness, due to thermal displacement of atoms, allowing collisions with smaller impact parameters (harder collisions) to occur. The translational energy lost by the incident molecule is transferred both to the lattice atoms of the surface and to internal energy of the incident molecule. The plot of the internal energy uptake as a function of the normal energy shows an initial rapid increase for small $E_{\perp}$, followed by a more gradual increase at higher $E_{\perp}$. The limit of the internal energy uptake is dictated by the molecular bond strength. The internal energy uptake by the molecules is greater for the 300 K surface than for the 0 K surfaces, consistent with the larger translational energy loss observed at the higher temperature.

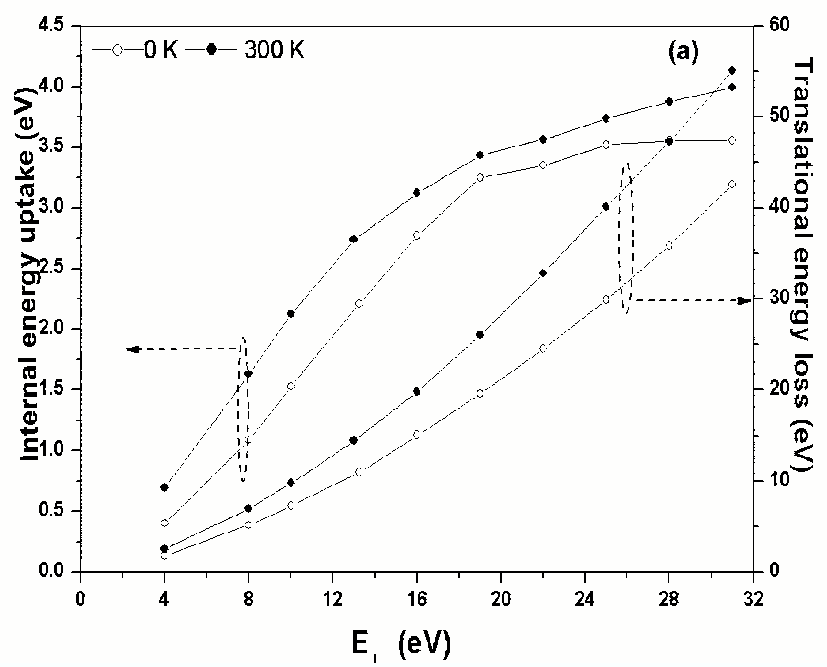

Figure 4(a): Average translational energy loss and average internal energy uptake as a function of $E_{\perp}$ for surviving CF.

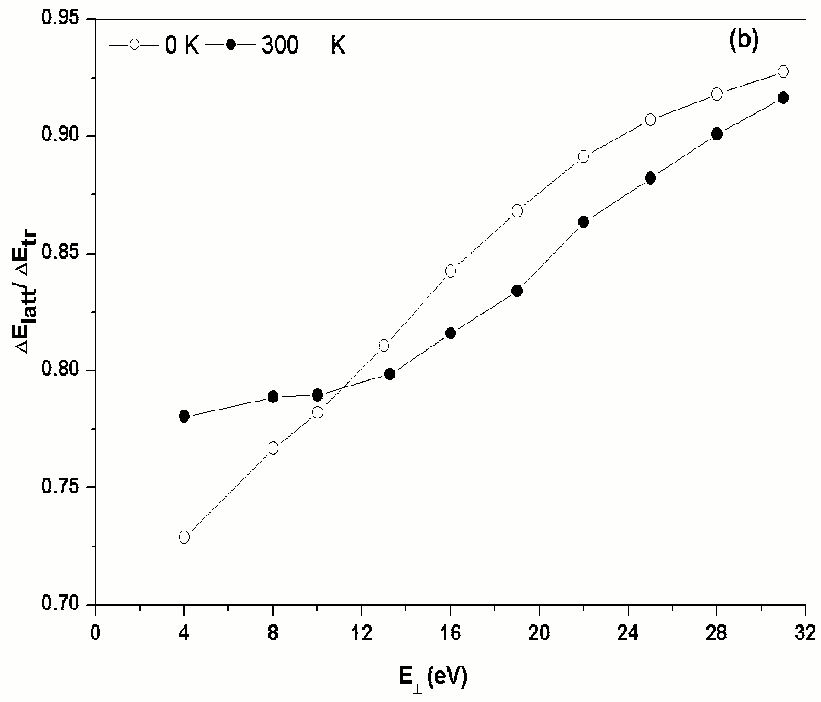

Figure 4(b): The fraction of the energy lost to the lattice atoms as a function of $E_{\perp}$ for surviving CF. Data shown for $E_{//}$ =1500 eV at surface

Figure 4(b) shows the fraction of the translational energy lost by the surviving molecules that is transferred to the lattice atoms as a function of the normal incidence energy at 0 K and at 300 K.

We note that the fraction transferred to the lattice atoms at 0 K varies from ~ 0.72 to ~0.92 as the normal incidence energy is increased from 4 eV to 31 eV. At 300 K the fraction varies form ~0.78 to ~0.93. Hence, in both cases, only a small fraction of the translational energy lost goes to the internal modes of the molecule. For relatively large normal incidence

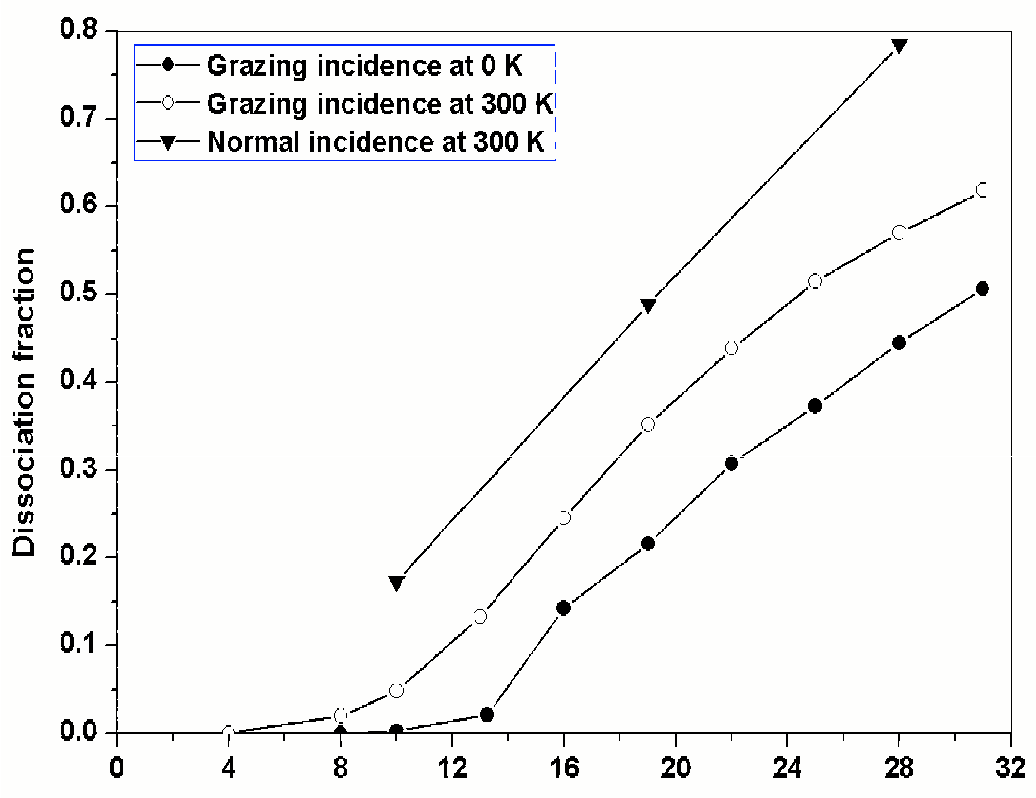

Figure 5: Dissociation fraction as a function of $E_{\perp}$ at surface temperatures of 0 K and 300 K for $E_{//}$ = 1500 eV; and at 300 K for $E_{//}$ = 0 eV.

energies ($E_{\perp}$ > 13 eV) the fraction transferred to the surface at 300 K follows the same trend as for 0 K. However, the absolute fraction is consistently lower for the room temperature surface, indicating a greater efficiency in the excitation of the molecule's internal modes compared to the 0 K surface. At more grazing incidence ($E_{\perp}$ < 13 eV), the fraction of translational energy that is transferred to the 300 K lattice becomes essentially constant at ~0.78. Hence, the redistribution of the translational energy between the surface atoms and the internal modes of the molecule has become independent of the normal energy/incidence angle in this region. A similar effect does not occur for the 0 K surface, indicating that it is a consequence of thermal motion of the surface atoms.

Molecules that gain internal energy (vibrational and/or rotational) as a result of a collision may subsequently dissociate [10]. Figure 5 shows the dissociation fraction of the scattered CF as a function of the normal incidence energy for the surface at 0 K and 300 K. At 0 K, there is a threshold for dissociation at $E_{\perp}$~12 eV, whereas for 300 K the threshold is at ~8 eV.

In both cases, the dissociation probability increases rapidly with increasing normal energy after the threshold. For a given normal energy, the dissociation fraction is consistently higher for the 300 K surface compared to the 0 K surface. This correlates with the larger translational energy loss and the larger internal energy uptake at 300 K observed in figure 4(a). Also shown on figure 5 are sample dissociation rates calculated for CF molecules incidence along the surface normal ($E_{//}$=0 eV) at 300 K. The data points show a similar trend to the grazing incidence data but are consistently higher. Thus, comparing molecules with different incident angles on the basis of their normal incidence energy is qualitatively valid, but not quantitatively reliable. The level of agreement between the grazing- and normal-incident molecules indicates that grazing incidence studies but utilized to gain information about low-energy molecular interaction with surfaces. Note that the total energy of the

grazing-incident molecules is substantially greater than that of the normal incident molecules, but that the dissociation rate is lower. The dissociation rate is directly related to the 'final' internal energy of the molecules. The lower dissociation rate for grazing incidence scattering is a consequence of additional molecule-surface interactions that occur as a result of the efficient excitation of rotational motion (see later).

Gerber and co-workers have suggested that I_2 molecules scattering from rigid surfaces dissociate once the rotational energy exceeds the bond energy of the molecule [28; 29]. In the work by van den Hoek and Kleyn it was concluded that initial rotational excitation is converted to vibrational energy resulting in the dissociation of O_2 molecules scattered from a rigid surface at normal incidence [10]. In order to investigate the mechanisms operative in the scattering of CF scattering at grazing incidence from the Si surface, we compared the internal energy and the rotational energy of the surviving molecules both at the turning point and after the collision. The turning point is defined as the point where the normal velocity of the molecule's CM is zero - corresponding to the point of the closest approach to the surface. At the turning point all incident molecules are still intact. Hence, in order to ensure valid comparison, we select only the subset molecules that are found to ultimately survive the collision when comparing the situation at turning point with that after the collision.

5.3.2 Redistribution of internal energy.

The averaged total internal energy (E_{int}) and averaged rotational energy (E_{rot}) of CF, both at the turning point (TP) and after collision, are shown in figure 6(a) as a function of $E_{\perp}$. The difference between these two energies represents the vibrational energy. At the turning point, both the internal energy and the rotational energy increase in a linear fashion with increasing $E_{\perp}$ across the full range studied. After the collision, the internal and rotational energies also initially increase as a function of the normal incidence energy, but then begin to plateau at $E_{\perp}$ ~20 eV. Both the rotational energy and the internal energy at the turning point are always greater than the corresponding energies after the collision. The averaged rotational energy at the turning point for $E_{\perp}$=31 eV is 3.73 eV. This is still less than the bond strength of 5.7 eV. Note however that some individual molecules that ultimately survive the collision have rotational energies that exceed the bond strength at this point. After the collision, the averaged rotational energy has decreases to 1.39 eV. There is always a net loss of rotational energy after the turning point for the energy range studied. Figure 6(b) shows the fraction E_{rot}/E_{int} (ratio of rotational energy to total internal energy) for surviving molecules both at the turning point and after the collision as a function of their respective internal energies. In both cases, the rotational fraction decreases with increasing total internal energy. The initial decrease (for low internal energies) is relatively rapid, followed by a more gradual decrease at higher internal energies. It is clear from figure 6(b) that, for a given total internal energy, rotational excitation is always the dominant component when the molecules is at the turning point, as Gerber and coworkers concluded [11]. In contrast, after the collision the relative importance of rotational versus vibrational excitation shows significant variation depending on the total internal energy, with vibrational excitation being dominant as the dissociation limit is approached.

When considering the rotational fractions shown in figure 6(b), an important distinction must be made between the curve for molecules at the turning point and the curve for molecules after the collision. The curve at the turning point represents a snapshot of the molecules in a non steady-state condition. Energy exchange by translational energy loss to the internal modes and/or the surface and energy redistribution between the internal modes of the molecules are still on-going processes at this point. In contrast, the curve for the surviving molecules after the collision is for a steady-state condition. The shape of this curve is ultimately defined by the atomic potentials. An ensemble of scattered molecule that is

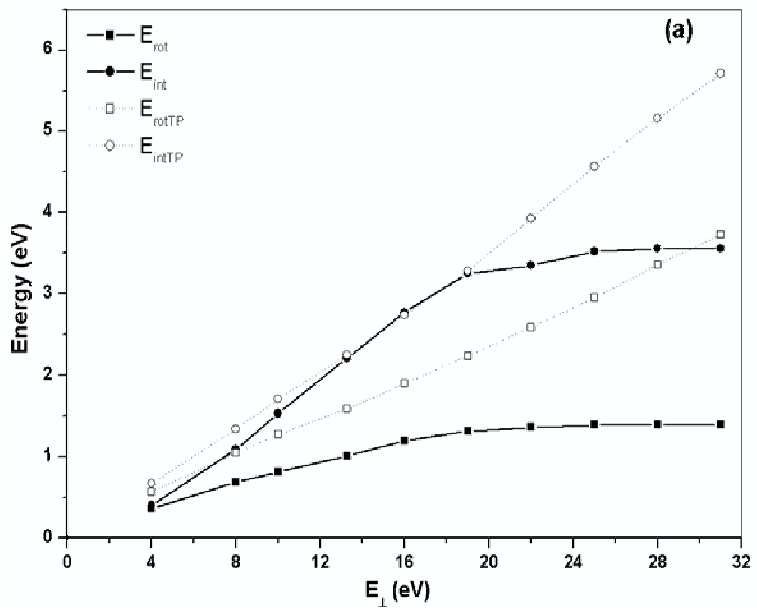

Figure 6(a): The internal and rotational energies at the turning point (open symbols) and after collision (filled symbols) as a function of the normal incidence energy for the surviving molecules.

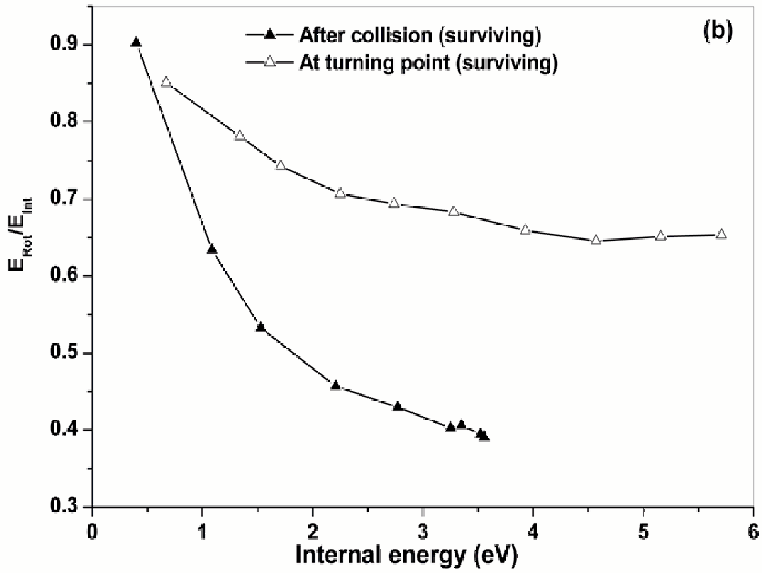

Figure 6(b): The rotational fraction at the turning point (open symbols) and after the collision (filled symbols) as a function of the internal energy for the surviving molecules. $E_{//}$=1500 eV and a surface temperature of 0 K

vibrationally and rotationally excited will distribute its total internal energy such that its rotational fraction will fall on the curve defined by the molecules after the collision shown on figure 6(b) (provided it is free of external influences). In this respect, the collision prior to the turning point with the surface serves only to provide the initial rotational and vibrational excitation and to determine the maximal internal energy of the molecule.

The molecules at the turning point can have an averaged internal energy that greatly exceed the bond strength because they are in a non-equilibrium state. In contrast, after the

collision all surviving molecules have an internal energy less than the bond strength. This upper limit is the origin of the plateaus seen in figures 4 (a) and 6(a), and the bunching of the data points seen in figure 6(b) (each data point corresponds to a specific initial normal incident energy). For the energy range studied there is no indication of an upper limit to the transient internal energy that can be present in the molecule at the turning point, although such a limit should emerge for higher normal incidence energies. Comparing the rotational fraction of the surviving molecules at the turning point with that of the same molecules after the collision shows that in most cases the final rotational fraction is significantly lower. At the turning point, the rotational fraction of the internal energy in the surviving molecules is always more than 65%. At very grazing incidence, the fraction reaches more than 80%. In contrast, after the collision the rotational fraction is less than 50 % for molecules whose internal energy exceeds ~1.5 eV. It is clear from figure 6(b) that if the total internal energy is low (corresponding to the low normal incident energy data points), the rotational mode will be dominant, whereas the vibrational mode becomes more important as the total internal energy increases. Molecules at the turning point have a significantly higher rotational excitation than is observed for molecules in the steady-state with the same total internal energy.

In figure 7(a), the fractions E_{vib}/E_{vibTP}, E_{rot}/E_{rotTP} and E_{int}/E_{intTP} are presented, where E_{vib}, Erot and E_{int} denote the final averaged vibrational, rotational energy and total internal energies after the collision, respectively, and E_{vibTP}, E_{rotTP} and E_{intTP} represent the same energies at the turning point. The fraction E_{vib}/E_{rot} for molecules, both at the turning point and after the collision, is presented in figure 7(b). These ratios offer an insight into the redistribution of internal energy during the latter half of the scattering event. Considering the energy ratios shown in figure 7(a), any value greater than 1 represents a net gain in energy between the turning point and the final far field, while a value less than 1 represents a net loss. In the case of the total internal energy ratio, it initially increases with increasing normal incidence energy, reaches a maximum and subsequently decreases again. The maximum value, which occurs at normal incidence energy of 16 eV, is 1. At this point there is (on average) no net gain or loss of internal energy by the molecules as they travel from the turning point to the region in which the interaction with the surface ceases. It should be stressed that this does not necessarily mean that there is no energy exchange between the individual molecules and the surface, only that the net effect of all energy exchanges on the averaged total internal energy of the molecules is zero after the turning point. In all other cases, there is a net loss of internal energy to the surface.

We can see from figure 7(a) that the rotational ratio is less than 1 across the full range of normal incident energies, indicating that in all cases there is a net loss of rotational energy between the turning point and the end of the collision process. In contrast, the vibrational ratio is greater than 1 for most incidence energies indicating a net gain during the latter half of the collision. The notable exception is for the most grazing incidence trajectory ($E_{\perp}$ = 4 eV) where there is also a net loss of vibrational energy.

Figure 7(a) can be divided into two regions: one for normal incidence energies less that 16 eV and the other for normal incidence energies greater than 16 eV. When reducing the normal energy from 16 eV (moving to the left on fig 7(a)), the rotational ratio remains effectively constant as a function of the normal energy. In this region, the rotational energy is reduced by about 38% during the latter half of the collision, irrespective of the normal incidence energy. In contrast, the vibrational ratio decreases dramatically with decreasing normal energy, moving from a net gain at the higher values to a net loss for the lowest normal energy calculated. This drop in the relative importance of the vibrational mode is also evident in figure 7(b), where the ratio of vibrational to rotational energy after the collision drops dramatically as $E_{\perp}$ is decreased from 16 eV. In comparison, the change in this ratio at the

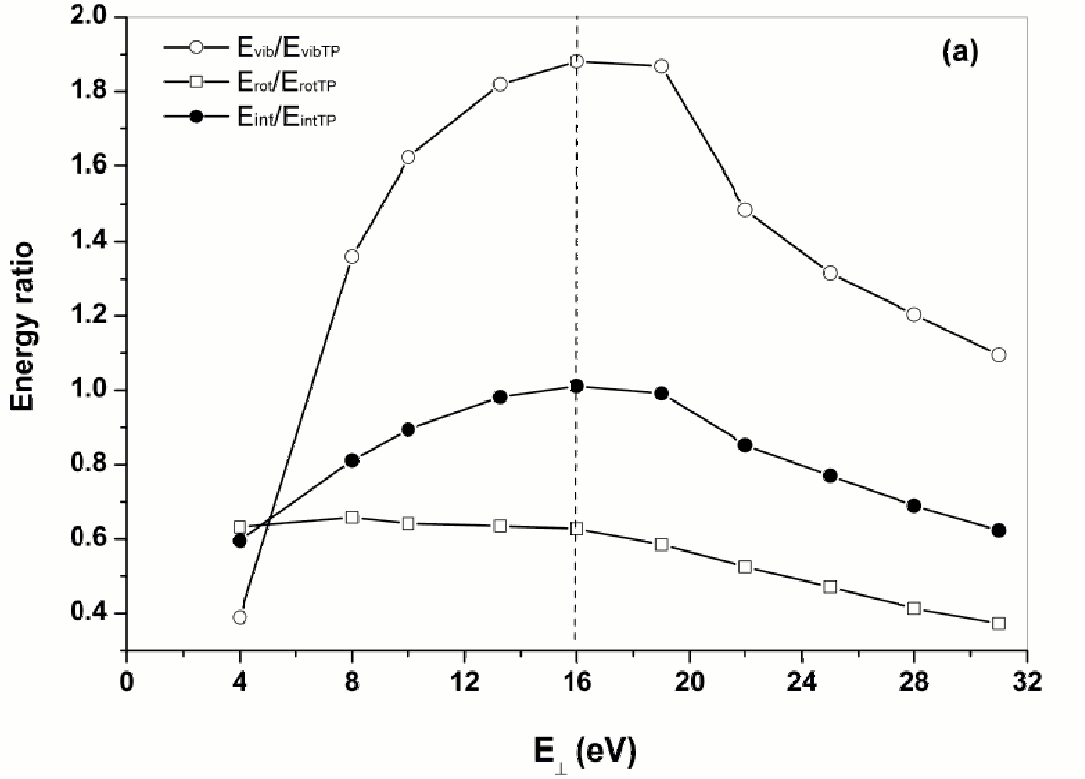

Figure 7(a): The fractions E_{rot}/E_{rotTP}, E_{vib}/E_{vibTP} and E_{int}/E_{intTP} as a function of the normal incidence energy for the surviving molecules. (b) The fraction E_{vib}/E_{rot}, as a function of the normal incidence energy at the turning point and after the collision for the surviving molecules. $E_{//}$=1500 eV and at a surface temperature of 0 K.

turning point as a function of $E_{\perp}$ is far less pronounced. The amount of vibrational excitation of the molecule at steady state is dependent on the total internal energy as shown in figure 6(b). With decreasing total internal energy, the fraction of the internal energy that can be accommodated in the vibrational mode decreases. To a lesser degree, the same is true of molecules at the turning point. As $E_{\perp}$ decreases, less of the rotational excitation gained at the turning point is converted to vibrational excitation at the steady state. For normal energies greater than 16 eV (moving to the right on fig. 7(a)) both the rotational fraction and the vibrational fraction decrease along with the decrease in the internal energy fraction. Figure 7(b) shows that the ratio of vibrational to rotational excitation in this region is independent of $E_{\perp}$ both at the turning point and after the collision. The absolute vibrational energy after the collision is greater than that at the turning point in this region ($E_{vib}/E_{vibTP} > 1.0$), even though the total internal energy of the molecules is decreasing (i.e. the molecules are still gaining vibrational energy between the turning point and the final equilibrium). In contrast, there is a net loss of rotational energy after the collision and the fraction lost increases with the normal incidence energy. The loss of rotational energy between the turning point and the steady state is a consistent feature across the full range of normal incidence energies. The gain in vibrational energy after the turning point can be attributed mainly to conversion from rotational excitation. This conversion occurs in competition with the loss of internal energy to the surface.

In order to illustrate the conversion dynamics between the rotational and vibrational modes after the turning point, we present their evolution for a single dissociating molecule (shown in figure 8(a)) and a single surviving molecule (shown in figure 8(b)).

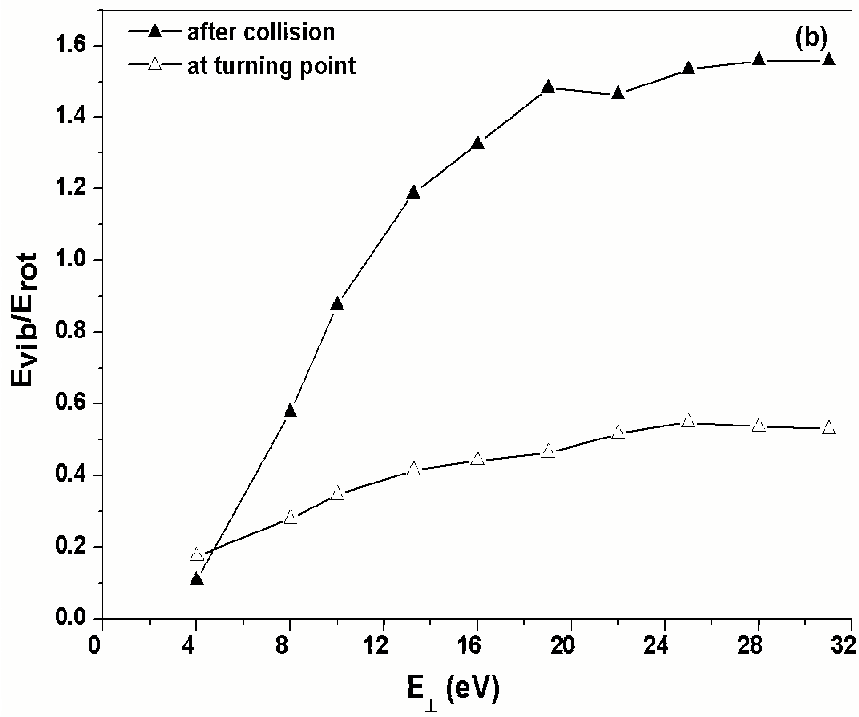

Figure 7(b): The fraction E_{vib}/E_{rot}, as a function of the normal incidence energy at the turning point and after the collision for the surviving molecules. $E_{//}$=1500 eV and at a surface temperature of 0 K.

The initial translational energy is 1531 eV ($E_{//}$= 1500 eV, $E_{\perp}$=31 eV). For the dissociating molecule, rotational excitation becomes evident at ~25 fs. At the turning point (33.5 fs), the rotational energy reaches a maximum value of 17.5 eV (more than three times the bond strength) and then decreases, while the vibrational energy increases continuously until dissociation. From the figure, we can determine that some of the initial rotational energy is transferred to vibrational excitation and some of it is transferred to the surface atoms. The energy exchange between the rotational motion and the surface atoms is evident from the oscillations that occur in the 35-60 fs region of the trajectory. Similar, but weaker, oscillations appear in the vibrational. Ultimately, dissociation results from the molecule gaining vibrational energy sufficient to overcome the bond strength. For the surviving molecule (figure 8(b)), there is simultaneous excitation of rotational and vibrational energies, although rotational excitation is the most dominant. At the turning point, the rotational energy reaches a maximum value of 11.5 eV (two times the bond strength). As before, after the turning point there is a large reduction in rotational energy and a corresponding increase in vibrational energy. Again, there are energy oscillations due to sequential interactions with the surface atoms. Ultimately, the molecule does not dissociate and after it has left the surface region there is a long-range oscillation of internal energy between the rotational and vibrational modes.

In order to highlight the role of the surface atoms in rotational energy transfer, identical trajectories are recalculated, but the interaction between the projectile and the surface atoms is removed once the turning point is reached. The results are shown in figure 8(c) for the dissociating molecule and figure 8(d) for the molecule that previously survived (but now also dissociates). By removing the interaction with surface atoms, we can clearly see that the rotational energy transfers completely to vibrational energy leading to dissociation. The decrease in the rotational energy after the turning point is slower in both figures 8(c) and (d) than it is in the corresponding curves in figures 8(a) and (b) and is completely smooth in the absence of a surface interaction. Hence, the redistribution of rotational energy is enhanced by

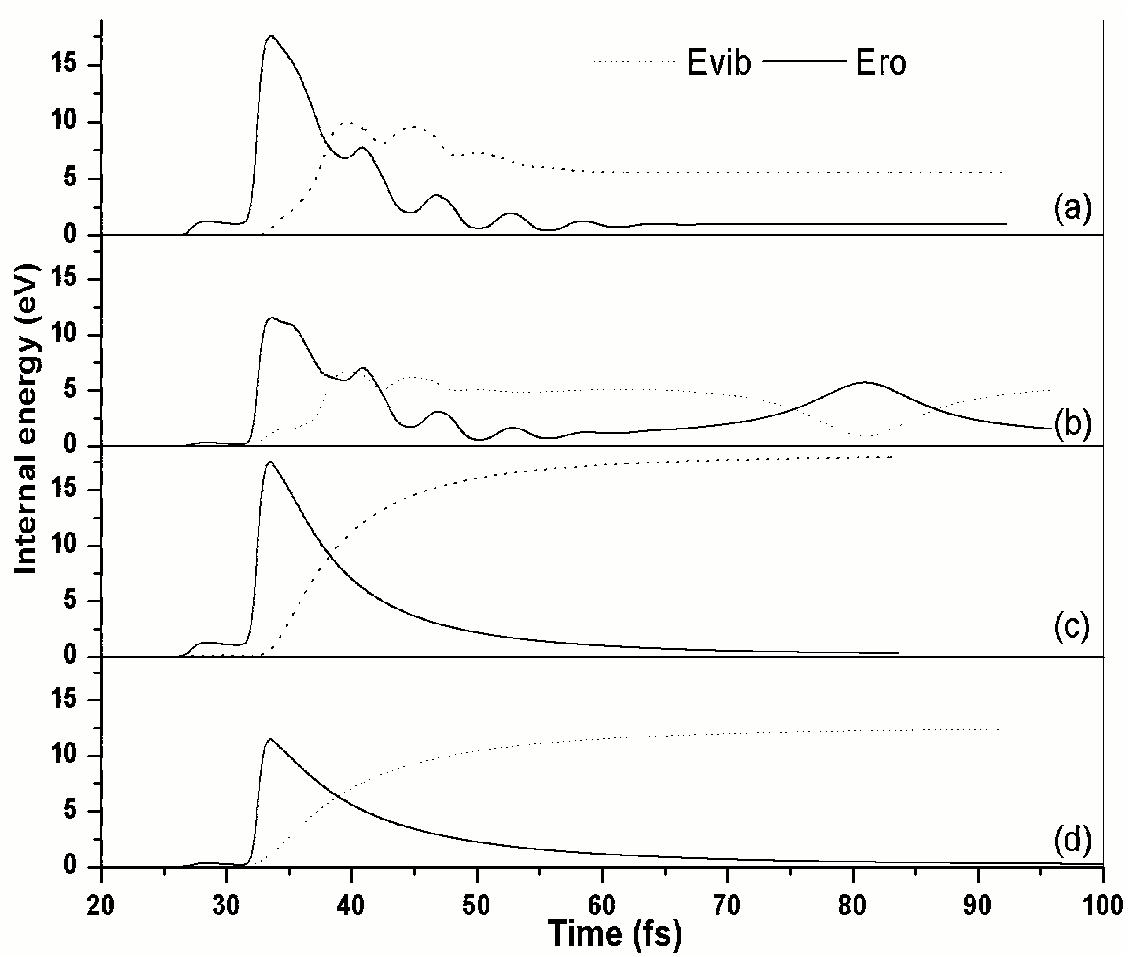

Figure 8: The evolution of the vibrational and the rotational energies for a dissociating molecule; (a) and a surviving molecule (b). After the removal of the surface interaction at the turning point, the evolution of the vibrational and the rotational energy for the same dissociating molecule (c) and the same "surviving" molecule (d).

the interaction with the surface atoms and it is clear that the oscillations in the rotational and vibrational energies seen on figure 8(a) and (b) result from interaction of the projectile with the surface atoms. By removing the surface interaction, the rotational energy, which is much larger than the bond strength at the turning point, remains in the molecule and results in dissociation. In both figure 8(c) and (d) the final "vibrational energy" is significantly higher than when the surface interaction is considered for the entirety of the collision. The main effect of the surface interactions after the turning point is to remove internal energy from the molecule, thus increasing the survival probability. Referring back to figure 2, the reason that the scattered atoms exhibit a smaller energy loss (at maximum) compared to the surviving molecules is now evident. The initial collisions of the molecules with the surface results in translational energy loss coupled with an internal energy uptake. However, after the initial strong excitation of the internal modes (primarily rotational), subsequent collisions allow for further translational energy loss coupled with a net loss of internal energy. Hence, molecules can lose more of their initial translational energy and simultaneously increase their survival probability. If there are few subsequent collisions, there is less loss of translational energy, but also less opportunity to reduce the initial large internal energy gain.

The behavior of CF differs from that of I_2 scattering from a flat surface [11], where I_2 molecules scattering from a flat surfaces dissociate if the rotational energy exceeds the bond

strength. In the case of a corrugated surface (current simulation), molecule can temporarily gain rotation energy in excess of the bond strength and still ultimately remaining intact because some of the rotational energy gained can be transferred to the surface atoms. It is evident from the energy oscillations seen on figures 8 (a) and (b) that there are multiple interactions between the incident molecules and atoms of the surface. Rotational energy is removed as a result of the chattering type collisions [30], indicated by the rapid oscillations observed on figures 8 (a) and (b) for collision times between 35 and 60 fs. This is a natural consequence of the grazing angle of incidence utilized. The mechanism is similar to Ar scattering from Si (100) [5], where the trajectory of the projectile is gradually changed by a series of progressively harder interaction with the surface atoms, although the situation for molecular scattering is more complex. Following the classical turning point of CF (based on the CM of the molecule) over the trajectory gives a smooth trace with a single minimum at the point of closest approach to the surface. However, the individual atoms of the molecule invariably come closer to the surface than the CM. Efficient excitation of molecular rotation results in the individual atoms of the molecule experiencing several close interactions with the Si surface while the molecular CM is moving away from the turning point. Unlike Ar scattering, where the interaction potential between the projectile and the surface tends to be symmetric about the turning point, the interaction potential between CF and the surface is highly asymmetric about the classical turning point due to rotational excitation. The strongest interaction occurs around the turning point, but due to rotational and vibrational motion, a greater number of (weaker) interactions occur during the latter half of the collision. The overall picture arising from figures 6-8 is one where the incident molecules initially experience strong rotational excitation around the classical turning point. After this point two competing processes occur involving the transfer of rotational energy either to vibrational excitation or to the atoms of the surface. Some direct vibrational excitation occurs as a result of the collision with the surface but the main mechanism by which translational energy is converted to internal energy is rotationally mediated. Similarly, loss of internal energy to the surface during the latter half of the collision is mainly via rotational de-excitation.

5.3.3 Stereodynamics

For the simulations the initial polar and azimuthal orientations of the incoming molecules were selected randomly with a uniform distribution and the molecules had no initial rotational or vibrational excitation. All molecules that survive the collision have some degree of vibrational and rotational excitation. In order to characterize the stereodynamic motion of the surviving molecules, the distribution of the polar angle of the rotational angular momentum (θ_J), is shown in figure 9(a) for $E_{//}$ = 1.5 keV, $E_{\perp}$ = 28 eV at 0 K. Here, the polar angle is defined with respect to the surface plane as shown in figure 1. The distribution of polar angles, is peaked around $\theta_J = 0$, indicating that the rotational planes of the molecules are preferentially aligned with the surface normal. If these molecules rotate such that the plane of rotation is the same as the scattering plane, then the motion can be characterized as "cart-wheel", whereas if the plane of rotation is perpendicular to the scattering plane (for θ_J=0°) the motion is "propeller"-like. The polar angle distribution shown in figure 9(a) has a minimum at θ_J=±90° indicating poor excitation of a "helicopter" like motion. In order to distinguish between cartwheel and propeller rotation of the scattered molecules, a contour diagram of the intensity distribution $I(\theta_J,\phi_J)$ is presented in figure 9(b). The azimuthal angle distribution (ϕ_J) is the angle of the projection of $\vec{J}$ onto the surface plane with respect to the initial incidence trajectory. Consequently, $\phi_J = 0^\circ$ corresponds to the $\vec{J}$ projection being parallel to the initial trajectory along the surface (propeller-like motion) and $\phi_J = \pm 90°$ corresponds to the $\vec{J}$ projection being perpendicular to the initial trajectory (cartwheel-like motion). From the

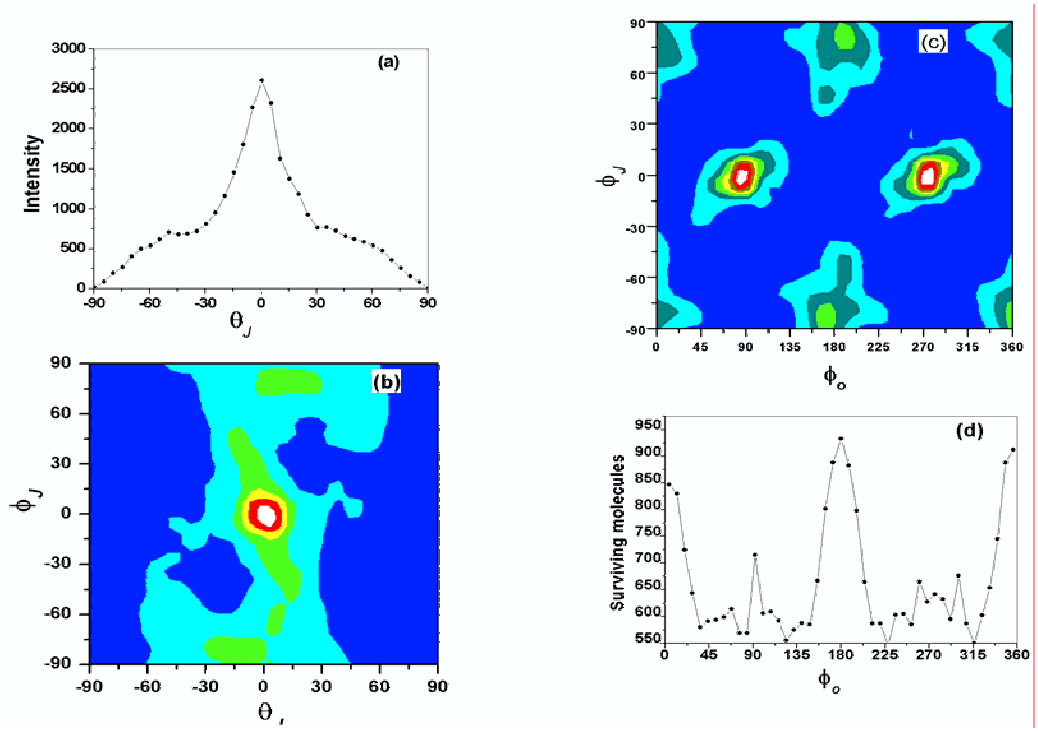

Figure 9: (a) The distribution of the polar angle of the rotational angular momentum (θ_J) of scattered CF molecules. **(b)** A contour diagram of the intensity distribution $I(\theta_J, \phi_J)$ (ϕ_J represents the azimuthal angle of the rotational angular momentum). **(c)** A contour diagram of the intensity distribution $I(\theta_J, \phi_o)$, where ϕ_o is the initial azimuthal orientation of the molecular axis. **(d)** The number of surviving molecules as a function of ϕ_o. $E_{//}$ = 1500 eV, $E_{\perp}$ = 28 eV at a surface temperature of 0 K.

contour diagram, two peaks are observed. The most intense peak is at θ_J =0° and ϕ_J = 0° corresponding to propeller-like motion. To our knowledge, this is the first prediction of propeller-like motion in molecular scattering from surfaces. A broader peak, located at θ_J =0° and ϕ_J = ±90°, is due to cartwheel-like motion. A contour diagram of the intensity distribution I(θJ,ϕo) is presented in figure 9(c) to illustrate the relationship between the initial azimuthal orientation of the molecular axis (ϕ_o) and the final motion of the surviving molecules. For molecules oriented parallel to the initial trajectory along [100] atomic rows (corresponding to 0°, 180° and 360° in the figure), the cartwheel-like motion is dominant. For molecules oriented perpendicular to the initial trajectory, the propeller-like motion is dominant. The number of surviving molecules as a function of the initial azimuthal orientation is shown in figure 9(d). Note that the maximum number of the surviving molecules is observed for the orientation that exhibits a cartwheel-like motion after scattering, while survival is significantly lower for orientation that yields a propeller-like rotation. However, the maximum intensity on the contour plots shown in figures 9(b) and (c) is due to the molecules with a propeller-like motion. The reason is that, although fewer molecules with a propeller-like motion survive the collision, those that do survive have a significantly narrower distribution of ϕ_J (better alignment with respect to each other). Figures 9(c) and (d) illustrate that the type of rotational motion observed is strongly dependent on the initial azimuthal orientation of the molecule, and that this also affects the survival probability. Similar analysis showed no dependence of the dissociation probability on the initial polar orientation of the molecules. It is clear that the molecular orientation with respect to the surface plays a role in the survival probability and the molecular motion. Consequently, we investigated whether the surface structure also influenced these properties. In Ar trajectory calculations under grazing

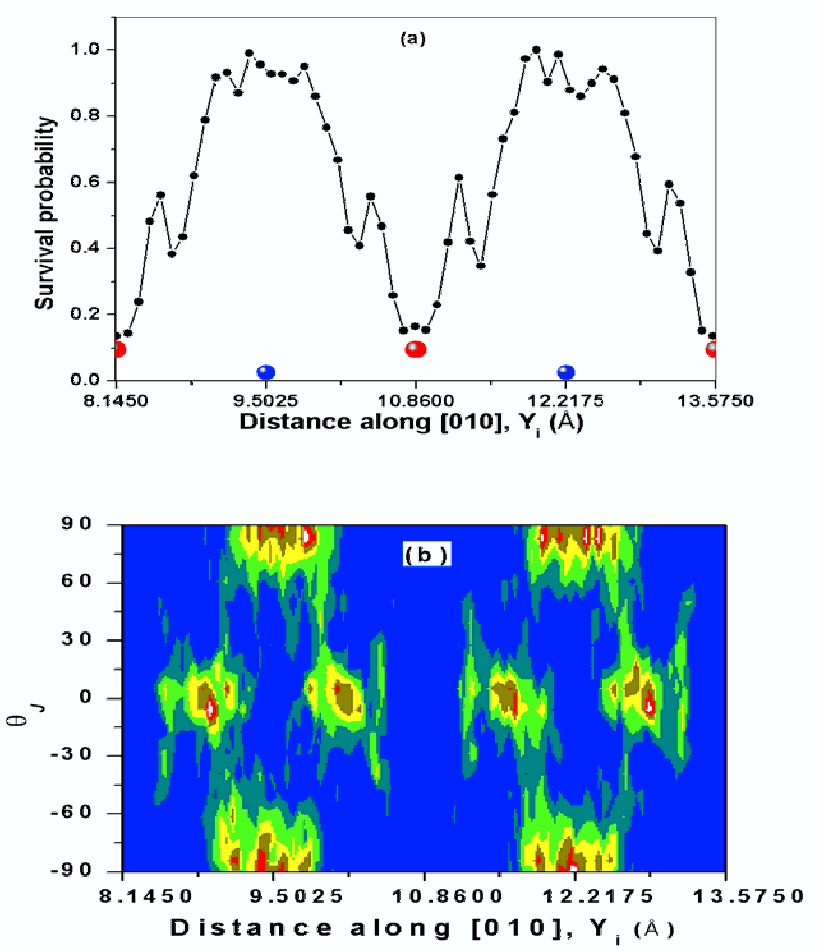

Figure 10: (a) Survival probability as a function of the initial Y component of the CM of the incident molecules (Y_I). **(b)** A contour diagram of the intensity distribution $I(Y_i, \phi_J)$. . $E_{//}$ = 1500 eV, $E_{\perp}$ = 28 eV at a surface temperature of 0 K.

incidence, it was found that the atoms undergo maximum translational energy loss when they impact just over the atomic rows of the first layer. Figure 10(a) shows the dependence of the survival probability on the initial Y-value of the CM of the molecules for $E_{//}$ = 1.5 keV, $E_{\perp}$ = 13 eV. The initial orientations of the incoming molecules are again chosen randomly with a uniform distribution. When the CM is aligned exactly with the atomic rows of first layer, the survival probability is less than 20%, consistent with the large energy loss observed for Ar scattering [5]. Molecules scattering from the first layer rows have the highest CM turning point. Such molecules have the lowest probability of further interaction with the surface atoms after the turning point and hence are less likely to be able to transfer internal energy back to the surface. When the CM is over the atomic rows of the second layer, almost no dissociation occurs. Comparing to the Ar scattering simulations, scattering from the second layer rows involves longer interaction times and weaker individual interactions with the surface atoms. This correlates with the higher survival probability observed for CF. Figure 10(b) shows a contour graph of the intensity distribution $I(Y_i, \theta_J)$. Here, Y_i denotes the initial CM component of the incident molecule. Due to the high dissociation probability of molecules with a CM aligned with the first layer atomic rows, there is a minimum in the contour plots at these points. From this figure, we can see that the cartwheel-type motion is dominant when the CM is aligned with the atomic rows of the second layer. These molecules are in effect scattering from the bottom of the 'valley' formed by the adjacent atomic rows of

the surface atoms. The propeller-type motion is dominant when the CM is between the atomic rows of the first and the second layers. This can be characterized as scattering from the 'valley' walls created by the first-layer atomic rows. From figure 10(b) it is evident that the bulk of the molecules exhibiting propeller-like motion scatter from points nearer to the second layer atoms (i.e. nearer the bottom of the 'valley' wall). These effects will be analyzed in greater detail in a subsequent paper.

5.4 Conclusion

Redistribution of internal energy during molecule-surface interactions is a complex and angle dependent process. In particular, at grazing incidence angles the maximum internal energy uptake during the collision process can be substantially larger than the final internal energy once the interaction with the surface ceases. Around the point of closest approach to the surface, the internal energy gain by the molecules is at a maximum. At grazing incidence there is always strong rotational excitation at this point. After the turning point the internal energy gained is redistributed both between the internal modes of the molecule and between the molecule and the surface atoms. Some of the rotational energy is converted to vibrational energy while the loss of internal energy to the surface is mainly mediated via the rotational mode. The ability to lose internal energy to the surface allows some molecules to temporarily gain internal energy far larger than the bond strength and yet still ultimately survive the collision.

In the current study, all surviving molecules were rotationally excited with their planes of rotation preferentially aligned with the surface normal. Both cartwheel- and propeller-like motion is evident in the rotation of the scattered molecules. The type of rotational motion can be correlated with the initial molecular orientation and the local atomic structure of the surface. Molecules whose axis is aligned with the initial trajectory along the surface have a higher probability of surviving the collisions. These molecules tend to exhibit cartwheel-like motion. In contrast, molecules whose axis is perpendicular to the initial trajectory have a lower survival probability and tend to exhibit propeller-like motion. Excitation of cartwheel like motion occurs predominantly from the bottom of channels formed by the first layer atomic rows, while propeller-like motion arises from collisions with the sides of these channels. Molecules with predominantly a propeller-like motion exhibit a significantly better alignment of their rotational planes (narrow $<\vec{J}>$ distribution) when compared with molecules with a pre-dominantly cartwheel-like motion.

The degree of dissociation as a function of $E_{\square}$ is comparable for $E_{//}$=1500 eV and $E_{//}$=0 eV (normal incidence). This clearly indicates that experiments at grazing incidence provide valuable details of dissociation dynamics and allow validation of computer models. The knowledge obtained can be used for better understanding of processes, such as plasma etching, in which this large parallel velocity is absent.

References

[1] J. P. Chang, J. W. Coburn, J. Vac. Sci. Technol. A 21 (2003) S145.
[2] G. R. Darling, S. Holloway, Rep. Prog. Phys. 58 (1995) 1595.

[3] W. Heiland, U. Imke, S. Schubert, K. J. Snowdon, Nucl. Instrum. Meth. B 27 (1987) 167.
[4] A. W. Kleyn, J. Phys.-Condens. Mat. 4 (1992) 8375.
[5] F. Gou, M. A. Gleeson, J. Villette, A. W. Kleyn, Nucl. Instrum. Meth. B 247 (2006) 244.
[6] T. Schlatholter, T. Schlatholter, M. Vicanek, W. Heiland, J. Chem. Phys. 106 (1997) 4723.
[7] P. J. Van den Hoek, T. C. M. Horn, A. W. Kleyn, Surf. Sci. 198 (1988) L335.
[8] P. H. F. Reijnen, P. J. Van den Hoek, A. W. Kleyn, U. Imke, K. J. Snowdon, Surf. Sci. 221 (1989) 427.
[9] H. Winter, Phys. Rep. 367 (2002) 387.
[10] P. J. Van den Hoek, A. W. Kleyn, J. Chem. Phys. 91 (1989) 4318.
[11] R. B. Gerber, A. Amirav, J. Phys. Chem. 90 (1986) 4483.
[12] J. S. Martin, B. T. Feranchak, J. R. Morris, J. N. Greeley, D. C. Jacobs, J. Phys. Chem. 100 (1996) 1689.
[13] J. C. Polanyi, R. J. Wolf, Ber. Bunsenges. Phys. Chem. 86 (1982) 356.
[14] W. R. Koppers, J. H. M. Beijersbergen, K. Tsumori, T. L. Weeding, P. G. Kistemaker, A. W. Kleyn, Phys. Rev. B 53 (1996) 11207.
[15] W. R. Koppers, K. Tsumori, J. H. M. Beijersbergen, T. L. Weeding, P. G. Kistemaker, A. W. Kleyn, Int. J. Mass. Spectrom. 174 (1998) 11.
[16] W. R. Koppers, M. A. Gleeson, J. Lourenco, T. L. Weeding, J. Los, A. W. Kleyn, J. Chem. Phys. 110 (1999) 2588.
[17] W. R. Koppers, J. H. M. Beijersbergen, T. L. Weeding, P. G. Kistemaker, A. W. Kleyn, J. Chem. Phys. 107 (1997) 10736.
[18] M. P. Allen, D. J. Tildesley, Computer Simulation of Liquids, New York, Oxford Science Publications, 1987.
[19] J. Tanaka, C. F. Abrams, D. B. Graves, J. Vac. Sci. Technol. A 18 (2000) 938.
[20] G. Molière, Z. Naturforsch 2a (1947) 133.
[21] R. J. W. E. Lahaye, A. W. Kleyn, S. Stolte, S. Holloway, Surf. Sci. 338 (1995) 169.
[22] P. M. Morse, E. C. G. Stueckelberg, Physical Review 33 (1929) 932.
[23] J. Tersoff, Phys. Rev. Lett. 61 (1988) 2879.
[24] J. Tersoff, Phys. Rev. B 38 (1988) 9902.
[25] J. Tersoff, Phys. Rev. B 39 (1989) 5566.
[26] K. Bruning, W. Heiland, T. Schlatholter, I. A. Wojciechowski, M. B. Medvedeva, V. K. Ferleger, J. Chem. Phys. 113 (2000) 2456.
[27] J. R. Peterson, Y. K. Bae, Phys. Rev. A 30 (1984) 2807.
[28] R. Elber, R. B. Gerber, J. Chem. Phys. 79 (1983) 4087.
[29] R. B. Gerber, L. H. Beard, D. J. Kouri, J. Chem. Phys. 74 (1981) 4709.
[30] J. N. Greeley, J. S. Martin, J. R. Morris, D. C. Jacobs, J. Chem. Phys. 102 (1995) 4996.